UAV-Assisted Time-Efficient Data Collection via Uplink NOMA

Wei Wang, *Graduate Student Member, IEEE,* Nan Zhao, *Senior Member, IEEE,* Li Chen, Xin Liu, *Senior Member, IEEE,* Yunfei Chen, *Senior Member, IEEE,* and Dusit Niyato, *Fellow, IEEE*

***Abstract*—Due to the mobility and line-of-sight conditions, unmanned aerial vehicle (UAV) is deemed as a promising solution to sensor data collection. On the other hand, it is vital to guarantee the timeliness of information for UAV-assisted data collection. In this paper, we propose a time-efficient data collection scheme, in which multiple ground devices upload their data to the UAV via uplink non-orthogonal multiple access (NOMA). The total flight time of the UAV is equally divided into N time slots. The duration of each time slot is minimized by jointly optimizing the straight-line trajectory, device scheduling, and transmit power. To solve this mixed integer non-convex optimization problem, we decompose it into two steps. In the first step, we study the device scheduling strategy based on the UAV trajectory and the channel gains between the UAV and ground devices, through which the original problem can be greatly simplified. In the second step, the duration of each time slot is minimized by optimizing the transmit power and the UAV trajectory. An iterative algorithm based on alternating optimization is proposed, where each subproblem can be alternatively solved by applying successive convex approximation with the device scheduling updated at the end of each iteration. Numerical results are presented to evaluate the effectiveness of the proposed scheme.**

***Index Terms*—Data collection, non-orthogonal multiple access, successive convex approximation, trajectory optimization, unmanned aerial vehicle.**

I. Introduction

Unmanned aerial vehicle (UAV) communication is a promising technology for future mobile networks, which has attracted wide interest recently due to its flexible deployment, high mobility, and favorable line-of-sight (LoS) conditions [2]. UAVs can work as aerial mobile users, which are integrated into cellular networks and served by ground base stations (BSs) [3], [4]. Mei *et al*. introduced a novel inter-cell interference coordination design in [3] to mitigate the strong uplink interference in cellular-connected UAV communication. In [4], Pang *et al*. investigated the uplink transmission in a cellular network from a UAV to its connected BS via non-orthogonal multiple access (NOMA). UAVs can also be quickly and efficiently deployed as aerial BS or relay to serve existing cellular networks and improve the quality of service (QoS) of ground users [5]–[7]. Lyu *et al*. investigated the placement of UAV-mounted mobile BSs in [5]. In [6], Gong *et al*. proposed a superimposed training-based two-phase robust channel estimation scheme for UAV-assisted cellular networks. In [7], Zhang *et al*. proposed a UAV-assisted mobile edge computing system, where the UAV is deployed as a mobile decode-and-forward relay.

On the other hand, with the tremendous utilization of the Internet of Things (IoT) devices, data collection becomes an important function in wireless sensor networks [8]. However, imprecise deployment leads to the disconnection of IoT devices in the remote areas or complex environment. Furthermore, UAV-assisted systems are expected to be an effective solution to this challenge [9]–[11]. The network energy efficiency and flight time minimization were investigated for wireless sensor networks by utilizing the UAV as a mobile data collector in [9] and [10], respectively. Samir *et al*. presented the UAV trajectory planning scheme for collecting data from time-constrained IoT devices with guaranteed performance in [11]. Different from conventional data collection systems, UAVs enable ground devices to transmit data to UAVs directly through LoS channels, leading to less energy consumption and higher transmission efficiency. In addition, UAVs can fly closer to the devices, adjust positions or even hover over them to achieve high QoS. Also, owing to the high flexibility, UAVs are more suitable for data collection in some emergency scenarios or infrastructure-free environments.

Despite the considerable benefits of UAV-assisted data collection, the limited flying time of UAV becomes a bottleneck in its applications. On the other hand, the large number of ground devices requires a long data uploading time. Therefore, within the limited flying time, it is important to improve the data collection efficiency. In this case, NOMA becomes an option [12], [13]. In power-domain NOMA, multiple users are allocated with different transmit power levels. Their signals are superimposed in the power domain and transmitted simultaneously. At the receiver, successive interference cancellation (SIC) is adopted to remove the multiple-access interference [14]. Owing to this, much research has been

Manuscript received August 27, 2020; revised January 24, 2021, March 22, 2021, May 24, 2021 and August 14, 2021; accepted August 15, 2021. The work was supported by the National Key R&D Program of China under Grant 2020YFB1807002, the National Natural Science Foundation of China (NSFC) under Grant 61871065, and the open research fund of State Key Laboratory of Integrated Services Networks under Grant ISN22-22. Part of this work is presented in IEEE WCNC 2021 [1]. The associate editor coordinating the review of this paper and approving it for publication was S. Ma. *(Corresponding author: Xin Liu.)*

conducted on UAV-assisted NOMA communications [15]–[23]. For example, Rupasinghe *et al*. introduced NOMA at UAV-BSs to serve more users simultaneously with millimeter-wave transmission and multi-antenna techniques in [15]. A novel scheme was proposed by Liu *et al*. to deal with the air-to-ground communication-assisted cooperative NOMA in [18]. In [19], Wang *et al*. presented a UAV-aided NOMA scheme to achieve secure wireless information and power transfer. Two schemes were proposed by Zhao *et al*. to guarantee the secure transmission in NOMA-UAV networks in [20]. A power allocation scheme with circular trajectory was proposed by Chen *et al*. for NOMA-UAV networks in [23] to maximize the sum rate of common users while guaranteeing the security for a specific user. Using NOMA, UAVs can serve multiple ground devices simultaneously for timely and efficient information gathering [24]–[29]. Nasir *et al*. proposed a UAV-enabled multiuser communication system, in which a single-antenna UAV-BS serves a large number of ground users by employing NOMA [25]. Hou *et al*. investigated the multiple antenna aided NOMA in UAV networks in [26]. The joint trajectory design and resource allocation were discussed by Cui *et al*. in [27] to maximize the minimum average rate among ground users for UAV networks utilizing both orthogonal multiple access (OMA) and NOMA. Zhao *et al*. proposed a UAV-assisted NOMA network, in which the UAV and BS cooperate to serve ground users simultaneously in [28]. The UAV mission completion time minimization problem in the ground-aerial uplink NOMA celluar networks was investigated by Mu *et al*. in [29].

The aforementioned research works have laid solid foundations on UAV-assisted NOMA networks. However, few research works have focused on uplink NOMA-UAV data collection [30]. Motivated by this, we propose a UAV-assisted data collection scheme via uplink NOMA. The main motivations and key contributions are summarized as follows.

- To the best of our knowledge, the investigation on the application of NOMA in UAV data collection is still in its infancy stage [30]. Thus, in this paper, we propose a joint optimization scheme for UAV-assisted uplink NOMA networks, which can achieve efficient data collection from ground devices. Different from [30], the UAV only allows a limited number of nearby devices to be connected to the uplink NOMA network in each time slot, leading to better LoS and easier SIC. The straight-line trajectory is optimized to enable all the ground devices to upload data to the UAV according to the device scheduling strategy.
- In the proposed scheme, the UAV flies straightly from the directly initial location to the destination to gather data from multiple ground devices via uplink NOMA. We formulate the time minimization problem based on the scheme by jointly optimizing the straight-line trajectory, device scheduling, and transmit power, under constraints on mobility and predefined data transmission threshold I_{th}. To solve this mixed integer non-convex optimization problem, we first propose a device scheduling strategy based on the straight-line trajectory and channel gains, which greatly simplifies the original problem.

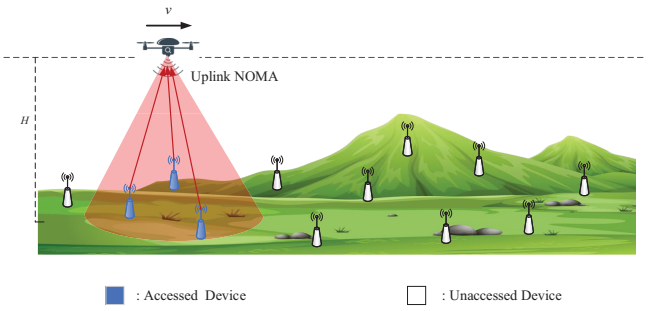

Fig. 1. UAV-assisted uplink NOMA network for data collection from K ground devices.

- Based on the device scheduling, the duration of each time slot can be optimized on UAV-assisted NOMA communications by two subproblems, i.e., the transmit power optimization and trajectory optimization. Each subproblem is first converted into a convex problem via successive convex approximation (SCA). Then, we propose an iterative algorithm based on alternating optimization to solve them alternatively with the device scheduling updated at the end of each iteration.

The rest of this paper is organized as follows. In Section II, the system model is presented, and the optimization problem is formulated with the device scheduling strategy. The approximation and optimization solutions to the joint optimization problem are demonstrated in Section III. In Section IV, simulation results are presented, followed by conclusions and future work in Section V.

Notation: Lower-case letters denote the scalars, vectors are denoted by black-body lowercase letters while black-body upper-case letters denote the real matrix. Curlicue letters are the column vector of matrix. $\mathbb{R}^{a\times b}$ is the $a\times b$-dimensional real matrix. $\mathcal{CN}(\mathbf{n},\mathbf{N})$ is the complex Gaussian distribution with mean matrix $\mathbf{n}$ and covariance matrix $\mathbf{N}$. $\mathbf{A}\succeq 0$ means that $\mathbf{A}$ is a Hermitian positive semidefinite matrix. $\bigtriangledown$ denotes the gradient, and $\frac{\partial^2 f}{\partial x^2}$ is the second order partial derivative of the function f with respect to variable x. For a vector $\mathbf{q}$, $\mathbf{q}^{\mathrm{T}}$ denotes its transpose and $\|\mathbf{q}\|$ is the Euclidean norm. $\mathrm{card}(\mathcal{A})$ denotes the cardinality of a set $\mathcal{A}$. The difference of sets $\mathcal{A}$ and $\mathcal{B}$ denotes as $\mathcal{A}-\mathcal{B}$.

II. System Model and Problem Formulation

In this section, the system model of UAV-assisted uplink NOMA networks for data collection is presented and the optimization problem is formulated.

A. System Model

As shown in Fig. 1, we consider a UAV-assisted uplink NOMA network, in which the UAV collects data from K ground devices. The devices are indexed by $\mathcal{K}=\{1,2,\ldots,K\}$, which are randomly distributed in a remote area. Each device has a fixed location $(\mathbf{u}_k^{\mathrm{T}},0)=(x_k,y_k,0)$. The UAV is deployed to fly straightly from an initial location $(\mathbf{q}_b^{\mathrm{T}},H)$ to the destination $(\mathbf{q}_e^{\mathrm{T}},H)$ with a constant altitude H, where $\mathbf{q}_b=(x_b,0)^{\mathrm{T}}$ and $\mathbf{q}_e=(x_e,0)^{\mathrm{T}}$. In each time slot, the UAV searches for the

nearby ground devices, allowing them to access the uplink NOMA network and send data to the UAV. Assume that all the devices have the same minimum data transmission threshold I_{th} (bit/Hz), i.e., the UAV should collect enough data from each ground device.

The goal is to minimize the total UAV flight time, and guarantee that the UAV can collect enough data from the devices. According to the time discretization (TD) method, we assume that the total flight time can be equally divided into N time slots as

$$T_{total} = N\Delta_t, \tag{1}$$

where Δ_t is the duration of each time slot, N should be chosen large enough such that Δ_t can be sufficiently small. As a result, the straight-line trajectory of UAV can be denoted as

$$\left(\mathbf{q}[n]^{\mathrm{T}}, H\right)^{\mathrm{T}} = (x_u[n], 0, H)^{\mathrm{T}}, n \in \mathcal{N} = \{1, 2, \ldots, N\}, \tag{2}$$

where $\mathbf{q}[n] = (x_u[n], 0)^{\mathrm{T}} \in \mathbb{R}^{2\times 1}$ is the horizontal location of the UAV in the nth time slot with

$$x_u[1] = x_b, \tag{3}$$

and

$$x_u[N] = x_e. \tag{4}$$

Furthermore, the mobility constraint of UAV can be expressed as

$$\left|x_u[n+1] - x_u[n]\right| \le V_{max}\Delta_t, \tag{5}$$

where V_{max} denotes the maximum speed of UAV. We have $V_{max}\Delta_t \le \varepsilon \ll H$, so that the distance between the UAV and each device is approximately unchanged and the speed of UAV is regarded as a constant within each time slot.

In this paper, we assume that the UAV flies in a straight line with fixed altitude. Thus, the distance between the UAV and the kth device in the nth time slot can be denoted as

$$d_k[n] = \sqrt{H^2 + \left(x_u[n] - x_k\right)^2 + y_k^2}, \quad \forall n, k. \tag{6}$$

The transmit power of the kth ground device in the nth time slot can be expressed as

$$0 \le P_k[n] \le P_{max}, \quad \forall n, k, \tag{7}$$

where P_{max} denotes the maximum transmit power for each ground device.

For convenience, we define a binary variable $\alpha_k[n] \in \{0, 1\}$ to denote the scheduling of the kth device for UAV in the nth time slot as

$$\alpha_k[n] = \{0, 1\}, \forall k \in \mathcal{K}, \forall n, \tag{8}$$

$$\sum_{k\in\mathcal{K}} \alpha_k[n] = S, \forall n, \tag{9}$$

where $\alpha_k[n] = 1$ indicates that the UAV allows the kth device to connect to the uplink NOMA network in the nth time slot, while $\alpha_k[n] = 0$ implies that the connection for the kth device is denied. In addition, S is the total number of accessible devices in each time slot based on design requirements.

According to the air-to-ground channel modeling [31], [32], the probability of LoS air-ground links can be written as

$$\mathbf{P}^{\mathrm{LoS}} = \frac{1}{1 + a_0 \exp\left(-b_0\left(\theta_k - a_0\right)\right)}, \tag{10}$$

where a_0 and b_0 are environmental constants. The elevation angle between the UAV and the kth device can be calculated as

$$\theta_k = \arctan\left(\frac{H}{\sqrt{\left(x_u[n] - x_k\right)^2 + y_k^2}}\right). \tag{11}$$

In the proposed scheme, the number of accessible devices in each time slot S is much less than the number of total devices K, i.e., $S \ll K$. Thus, the S closest devices to the UAV are scheduled to upload their data in each time slot, which makes the LoS probability always close to 1 during the flight when the altitude H is high enough according to (10) and (11). Thus, we assume that the communication links between the UAV and ground devices are dominated by LoS links and the channel gain only depends on the UAV-device distance. Furthermore, the Doppler effect caused by the UAV mobility is assumed to be well compensated. Accordingly, the channel gain between the UAV and the kth device in the nth time slot can be expressed as

$$h_k[n] = \sqrt{\frac{\beta_0}{H^2 + \left(x_u[n] - x_k\right)^2 + y_k^2}}, \quad \forall n, k, \tag{12}$$

where β_0 is the channel power gain at the reference distance of 1 meter.

We further define the access matrix for all the time slots as

$$\mathbf{M} = (M_i^n)_{S\times N} = \begin{bmatrix} M_1^1 & M_1^2 & \ldots & M_1^N \\ M_2^1 & M_2^2 & \ldots & M_2^N \\ \ldots & \ldots & \ldots & \ldots \\ M_S^1 & M_S^2 & \ldots & M_S^N \end{bmatrix}, \tag{13}$$

where the nth column denotes the access group in the nth time slot as $\mathcal{M}^n = \{M_1^n, M_2^n, \ldots, M_S^n\} \subseteq \mathcal{K}$, in which the accessible devices are sorted increasingly by the distances from the UAV as

$$d_{u,M_1^n}[n] \le d_{u,M_2^n}[n] \le \cdots \le d_{u,M_S^n}[n]. \tag{14}$$

Thus, the UAV allows the devices to access the NOMA network according to (13). The scheduling of the lth device in the nth time slot can be set as

$$\begin{cases} \alpha_l[n] = 1, & l \in \mathcal{M}^n, \\ \alpha_l[n] = 0, & \text{otherwise}. \end{cases} \tag{15}$$

The received superimposed messages at the UAV via uplink NOMA in the nth time slot can be expressed as

$$y[n] = \sum_{i=1}^{S} \sqrt{P_{M_i^n}[n]} h_{M_i^n}[n] s_{M_i^n}[n] + n_u, \forall M_i^n \in \mathcal{M}^n, \tag{16}$$

where $s_{M_i^n}[n]$ is the transmitted signal from the M_i^nth device with $\left|s_{M_i^n}[n]\right|^2 = 1$, and $n_u \sim \mathcal{CN}(0, \sigma^2)$ denotes the additive white Gaussian noise (AWGN) at the UAV, with zero mean and variance σ^2.

The UAV employs SIC to eliminate the multi-access interference based on different power levels and decode the messages from different users. In the uplink NOMA, the information of a user with higher channel gain is usually first decoded to maximize the sum rate [33], [34]. Thus, the SIC order at the UAV is the same as (14), i.e., from M_1^n to M_S^n. The received signal-to-interference-plus-noise (SINR) of the M_i^nth device, $1 \le i \le S-1$, at the UAV in the nth time slot can be expressed as

$$\gamma_{M_i^n} = \frac{P_{M_i^n}[n] \left|h_{M_i^n}[n]\right|^2}{\sum_{j=i+1}^{S} P_{M_j^n}[n] \left|h_{M_j^n}[n]\right|^2 + \sigma^2}. \tag{17}$$

For simplicity, we define

$$\hat{h}^2_{M_i^n}[n] = \frac{\left|h_{M_i^n}[n]\right|^2}{\sigma^2} = \frac{\rho_0}{H^2 + \left(x_u[n] - x_{M_i^n}\right)^2 + y^2_{M_i^n}}, \tag{18}$$

where $\rho_0 = \frac{\beta_0}{\sigma^2}$. Then, the received SINR in (17) can be rewritten as

$$\gamma_{M_i^n} = \frac{P_{M_i^n}[n]\hat{h}^2_{M_i^n}[n]}{\sum_{j=i+1}^{S} P_{M_j^n}[n]\hat{h}^2_{M_j^n}[n] + 1}. \tag{19}$$

Particularly, for the M_S^nth device, the received SINR at the UAV can be denoted as

$$\gamma_{M_S^n} = P_{M_S^n}[n]\hat{h}^2_{M_S^n}[n]. \tag{20}$$

Therefore, the achievable transmission rate from the M_i^nth device to the UAV in the nth time slot in bit/second/Hertz is given by

$$R_{M_i^n}[n] = \log_2\left(1 + \gamma_{M_i^n}\right), i \in \mathcal{S} = \{1, 2, \ldots, S\}. \tag{21}$$

Remark 1: (1) In the proposed scheme, the number of accessible devices S in each time slot is usually much less than the total number of ground devices K, which leads to higher probability of LoS links. In addition, $S \ll K$ reduces the error accumulation and complexity for SIC, which makes it more practical.

(2) The SIC order depends on the difference of channel gain. It is worth noticing that the channel quality between the UAV and each device is varying during the flight. Thus, the SIC order is always changing, and the achievable rate of devices is difficult to obtain. To solve it, we define $\mathcal{M}^n$ to present the SIC order in the nth time slot, and the instantaneous rate of each device can be obtained by $R_{M_i^n}[n]$ in (21).

B. Problem Formulation

Both path discretization (PD) and TD can be used to solve the trajectory design problem. For the PD scheme [29], [35], [36], its basic idea is to divide the continuous UAV trajectory into N consecutive line segments connected by a huge number of discrete points, while the time duration denoted as $\{t_n, \forall n\}$ that the UAV spends on can be different. As such, PD can be regarded as a more general case of TD by allowing unequal time-slot lengths over different line segments. Thus, PD can also be applied to the total flight time minimization problem. However, compared to the TD scheme, more design variables, i.e., $\{\mathbf{X}\}$, $\{\mathbf{A}\}$, $\{\mathbf{P}\}$ and $\{t_n, \forall n\}$, are coupled together, making the PD scheme much more complex and difficult to obtain its feasible solution. In addition, the TD scheme is still suitable by tuning the value of N if the total flight time itself needs to be optimized. Thus, we choose the TD scheme in this paper. To guarantee the effectiveness of data collection, we minimize the duration of each time slot Δ_t[1] by jointly optimizing the device scheduling $\mathbf{A} = \{\alpha_k[n], \forall k \in \mathcal{K}, \forall n \in \mathcal{N}\}$, the UAV straight trajectory $\mathbf{X} = \{x_u[n], \forall n \in \mathcal{N}\}$ and the transmit power $\mathbf{P} = \{P_k[n], \forall k \in \mathcal{K}, \forall n \in \mathcal{N}\}$, with predefined I_{th}. The optimization problem can be formulated as

$$\min_{\mathbf{P},\mathbf{X},\mathbf{A},\Delta_t} \quad \Delta_t \tag{22a}$$

$$s.t. \quad \sum_{k=1}^{K} \alpha_k[n] = S, \forall k \in \mathcal{K}, \tag{22b}$$

$$\sum_{n=1}^{N} \alpha_k[n] R_k[n] \Delta_t \ge I_{th}, \forall k \in \mathcal{K}, \tag{22c}$$

$$x_u[1] = x_b, x_u[N] = x_e, \tag{22d}$$

$$\left|x_u[n+1] - x_u[n]\right| \le V_{max}\Delta_t, n \in \mathcal{N} - \{N\}, \tag{22e}$$

$$0 \le P_k[n] \le P_{max}, \quad \forall n \in \mathcal{N}, k \in \mathcal{K}. \tag{22f}$$

Before the flight, the solution to (22) should be calculated offline by the ground station, which is then fed back to the UAV. At the beginning of the flight, the UAV first sends the solution to the close devices, which is then broadcast to other devices via an ad-hoc network. Thus, the devices can determine the transmit power and when to transmit in a distributed way. Note that this optimization problem is non-convex due to the non-convex constraints and the binary variables $\alpha_k[n]$, which is difficult to solve directly.

C. Device Scheduling Strategy

The binary variables in (22) makes the problem a mix-integer programming. Thus, we propose a device scheduling strategy according to the varying channel gains between UAV and ground devices to tackle it. In the proposed scheme, the UAV selects S devices to access the uplink NOMA network in each time slot, and there would be $\binom{K}{S}$ choices. When $K \gg S$, its complexity increases rapidly. In addition, it is necessary to guarantee that each device can deliver more than I_{th} bit/Hz to the UAV. Thus, we should perform the selection properly in each time slot. As mentioned above, we utilize $\mathbf{M}$ to simplify this problem, which is obtained based on the UAV trajectory and the varying channel gains between the UAV and ground devices.

According to *Remark 1*, the varying decoding order leads to the difficulty in calculating the instantaneous rate of each device. Thus, based on (15), we utilize $\mathbf{M}$ in (13) to replace $\mathbf{A}$, and introduce auxiliary sets as $\mathcal{W}_k = \{(i,n) | M_i^n = k, \forall i \in$

[1]When the optimized Δ_t^* is not sufficiently small to satisfy $V_{max}\Delta_t^* \le \varepsilon \ll H$, we can increase N to further minimize Δ_t^*.

$\mathcal{S}, \forall n \in \mathcal{N}\}, \forall k \in \mathcal{K}$. Then, the optimization problem in (22) can be changed into

$$\min_{\mathbf{P},\mathbf{X},\mathbf{M},\Delta_t} \quad \Delta_t \tag{23a}$$

$$s.t. \quad \sum_n R_{M_i^n}[n]\Delta_t \geq I_{th}, (i,n) \in \mathcal{W}_k, \forall k \in \mathcal{K}, \tag{23b}$$

$$x_u[1] = x_b, x_u[N] = x_e, \tag{23c}$$

$$\left|x_u[n+1] - x_u[n]\right| \leq V_{max}\Delta_t, n \in \mathcal{N} - \{N\}, \tag{23d}$$

$$0 \leq P_{M_i^n}[n] \leq P_{max}, \forall i \in \mathcal{S}, \forall n \in \mathcal{N}. \tag{23e}$$

$\mathbf{M}$ is an $S \times N$ matrix, in which each element represents the accessible device and the columns denote the varying SIC order over time slots. Thus, we proposed an effective device scheduling strategy to determine the devices to access the uplink NOMA network in each time slot, summarized as Algorithm 1.

Algorithm 1 Device scheduling strategy

1: Initialization: Fix the accessible number of devices S, and initialize the access matrix $\mathbf{M}$. For a given trajectory $\mathbf{X}$, and set the time slot $n = 1$.
2: **Repeat**
3: For $x_u[n]$, calculate the distances of devices from UAV by (6), and get the optimal access group $\mathcal{M}^{n*}$, which are sorted in an ascending order of distances.
4: Set device scheduling $\{\alpha_l[n] = 1, l \in \mathcal{M}^{n*}\}$; while $l \notin \mathcal{M}^{n*}$, set them to zero.
5: $n = n + 1$.
6: **Until** The maximum number of time slots N is satisfied.
7: Output: $\mathbf{M}^* = \{\mathcal{M}^{1*}, \mathcal{M}^{2*}, \ldots, \mathcal{M}^{N*}\}$.

In Algorithm 1, the access matrix $\mathbf{M}$ is closely related with the UAV trajectory $\mathbf{X}$. Thus, $\mathbf{M}$ changes with $\mathbf{X}$. Through Algorithm 1, the optimal $\mathbf{M}^*$ can be obtained for given UAV trajectory $\mathbf{X}$. Thus, the optimization problem can be simplified based on Algorithm 1 as

$$\min_{\mathbf{P},\mathbf{X},\Delta_t} \quad \Delta_t \tag{24a}$$

$$s.t. \quad M_i^n \in \mathbf{M}^*, i \in \mathcal{S}, n \in \mathcal{N}, \tag{24b}$$

$$\sum_n R_{M_i^n}[n]\Delta_t \geq I_{th}, (i,n) \in \mathcal{W}_k, \forall k \in \mathcal{K}, \tag{24c}$$

$$x_u[1] = x_b, x_u[N] = x_e, \tag{24d}$$

$$\left|x_u[n+1] - x_u[n]\right| \leq V_{max}\Delta_t, n \in \mathcal{N} - \{N\} \tag{24e}$$

$$0 \leq P_{M_i^n}[n] \leq P_{max}, \forall i \in \mathcal{S}, \forall n \in \mathcal{N}. \tag{24f}$$

However, due to the complexity of $R_{M_i^n}[n]$, the problem in (24) is still non-convex and cannot be solved directly. Thus, it is decomposed into two subproblems in the next section and solved iteratively. After each iteration, the suboptimal trajectory can be obtained, and $\mathbf{M}^*$ is updated by Algorithm 1 accordingly.

III. Joint Optimization of Power and Trajectory

In this section, we propose an effective algorithm to solve the optimization problem in (24). First, we decompose it into two subproblems. Then, the non-convex constraints are transformed into convex ones by applying SCA approximations. Finally, it is solved via alternating optimization.

A. Subproblem 1: Transmit Power Optimization

For a given UAV trajectory $\mathbf{X}$, the optimization problem in (24) can be decomposed as

$$\mathbf{P1}: \min_{\mathbf{P},\Delta_t} \quad \Delta_t \tag{25a}$$

$$s.t. \quad M_i^n \in \mathbf{M}^*, i \in \mathcal{S}, n \in \mathcal{N}, \tag{25b}$$

$$\sum_n R_{M_i^n}[n]\Delta_t \geq I_{th}, (i,n) \in \mathcal{W}_k, \forall k \in \mathcal{K}, \tag{25c}$$

$$0 \leq P_{M_i^n}[n] \leq P_{max}, \forall i \in \mathcal{S}, \forall n \in \mathcal{N}. \tag{25d}$$

P1 is difficult to solve due to the non-convex constraint (25c). We exploit SCA to make it convex.

First, according to $\mathbf{M}^*$ by Algorithm 1, (25c) can be tightened as

$$R_{M_i^n}[n] \geq \zeta \frac{I_{th}}{\mathrm{card}(\mathcal{W}_{M_i^n})\Delta_t}, M_i^n \in \mathcal{M}^{n*}, \forall n \in \mathcal{N}. \tag{26}$$

where ζ denotes a relaxation factor.

To simplify it, we first introduce some auxiliary variables as $\{m_{M_i^n}[n], M_i^n \in \mathcal{M}^n\}$ with

$$R_{M_i^n}[n] \geq m_{M_i^n}[n]. \tag{27}$$

Then, the inequality in (26) can be replaced by the following constraint.

$$m_{M_i^n}[n] \geq \zeta \frac{I_{th}}{\mathrm{card}(\mathcal{W}_{M_i^n})\Delta_t}. \tag{28}$$

Due to the fact that $\frac{1}{\Delta_t}$ is a convex function with respect to Δ_t when $\Delta_t > 0$, (28) can be transformed into a convex one as

$$\frac{1}{\Delta_t} \leq \frac{m_{M_i^n}[n]\mathrm{card}(\mathcal{W}_{M_i^n})}{\zeta I_{th}}, M_i^n \in \mathcal{M}^{n*}, \forall n \in \mathcal{N}. \tag{29}$$

Thus, the optimization problem in (25) can be revised as

$$\min_{\mathbf{P},\Delta_t} \quad \Delta_t \tag{30a}$$

$$s.t. \quad M_i^n \in \mathbf{M}^*, i \in \mathcal{S}, n \in \mathcal{N}, \tag{30b}$$

$$R_{M_i^n}[n] \geq m_{M_i^n}[n], M_i^n \in \mathcal{M}^{n*}, \tag{30c}$$

$$\frac{1}{\Delta_t} \leq \frac{m_{M_i^n}[n]\mathrm{card}(\mathcal{W}_{M_i^n})}{\zeta I_{th}}, M_i^n \in \mathcal{M}^{n*}, n \in \mathcal{N}, \tag{30d}$$

$$0 \leq P_{M_i^n}[n] \leq P_{max}, \forall i \in \mathcal{S}, \forall n \in \mathcal{N}. \tag{30e}$$

Problem (30) is still non-convex owing to the non-convex constraint (30c). To handle it, we first rewrite it as

$$\log_2\left(1 + \frac{\dfrac{\rho_0 P_{M_i^n}[n]}{H^2 + \left(x_u[n] - x_{M_i^n}\right)^2 + y_{M_i^n}^2}}{\displaystyle\sum_{j=i+1}^{S} \frac{\rho_0 P_{M_j^n}[n]}{H^2 + \left(x_u[n] - x_{M_j^n}\right)^2 + y_{M_j^n}^2} + 1}\right) \geq m_{M_i^n}[n]. \tag{31}$$

Then, based on SCA, we further introduce auxiliary variables $\{z_{M_i^n}[n], v_{M_i^n}[n], \forall M_i^n \in \mathcal{M}^{n*}\}$, and (31) can be approximated as

$$\frac{\rho_0 P_{M_i^n}[n]}{H^2 + \left(x_u[n] - x_{M_i^n}\right)^2 + y_{M_i^n}^2} \geq e^{z_{M_i^n}[n]}, \tag{32}$$

$$1 + \sum_{j=i+1}^{S} \frac{\rho_0 P_{M_j^n}[n]}{H^2 + \left(x_u[n] - x_{M_j^n}\right)^2 + y_{M_j^n}^2} \leq e^{v_{M_i^n}[n]}, \tag{33}$$

$$\log_2\left(1 + e^{z_{M_i^n}[n] - v_{M_i^n}[n]}\right) \geq m_{M_i^n}[n]. \tag{34}$$

Note that the constraints (32)-(34) are still non-convex. Thus, we introduce the Taylor series approximation and Proposition 1 to transform (32) and (33) into convex ones.

For a differentiable convex function $f(x)$, it can be approximated by its tangential function as $g(x, \bar{x})$, where $g(x, \bar{x})$ is the first order Taylor expansion around $\bar{x}$. Thus, we have

$$f(x) \geq g(x, \bar{x}) = f(\bar{x}) + \bigtriangledown f(\bar{x})(x - \bar{x}). \tag{35}$$

When $x = \bar{x}$, the equality holds.

Proposition 1: Define a function as

$$G(x) = e^x, \forall x \in \mathbb{R}. \tag{36}$$

The first order Taylor approximation to $G(x)$ around $\bar{x}$ can be expressed as

$$\mathcal{G}(x, \bar{x}) = e^{\bar{x}}(x - \bar{x} + 1). \tag{37}$$

In this way, $G(x)$ can be replaced by $\mathcal{G}(x, \bar{x})$.

Proof: The second order derivation of $G(x)$ is

$$\frac{\partial^2 G}{\partial x^2} = e^x \geq 0. \tag{38}$$

Hence, $G(x)$ is convex with respect to x. According to the Taylor series approximation, it satisfies the following inequality with any given $\bar{x}$.

$$G(x) \geq \mathcal{G}(x, \bar{x}) = e^{\bar{x}}(x - \bar{x} + 1). \tag{39}$$

Similarly, the approximation in (39) holds with the conditions $x = \bar{x}$ satisfied. Thus, from the above derivation, (36) can be replaced by (37). ∎

According to Proposition 1, substituting auxiliary variables $\{z_{M_i^n}[n], v_{M_i^n}[n]\}$ into (37) based on the law of derivation, we have

$$\frac{\rho_0 P_{M_i^n}[n]}{H^2 + \left(x_u[n] - x_{M_i^n}\right)^2 + y_{M_i^n}^2} \geq e^{\bar{z}_{M_i^n}[n]}\left(z_{M_i^n}[n] - \bar{z}_{M_i^n}[n] + 1\right), \tag{40}$$

$$1 + \sum_{j=i+1}^{S} \frac{\rho_0 P_{M_j^n}[n]}{H^2 + \left(x_u[n] - x_{M_j^n}\right)^2 + y_{M_j^n}^2} \leq e^{\bar{v}_{M_i^n}[n]}\left(v_{M_i^n}[n] - \bar{v}_{M_i^n}[n] + 1\right). \tag{41}$$

Therefore, the constraints (32) and (33) can be replaced by (40) and (41), which are approximated as convex ones.

Then, (34) is non-convex. Although it can be transformed to convex by simply taking exponential at both sides, it cannot be solved effectively via CVX [37]. Thus, we introduce Proposition 2 to approximate it.

Proposition 2: Define a bivariate function as

$$F(x, y) = \log_2(1 + e^{x - y}), \tag{42}$$

where $\forall x, y \in \mathbb{R}$. The first order Taylor approximation to $F(x, y)$ around $(\bar{x}, \bar{y})$ can be expressed as

$$\begin{aligned} \mathcal{F}(\bar{x}, \bar{y}) = &\log_2\left(1 + e^{\bar{x} - \bar{y}}\right) \\ &+ \frac{e^{\bar{x} - \bar{y}}}{(1 + e^{\bar{x} - \bar{y}})\ln 2} \times (x - \bar{x} - y + \bar{y}). \end{aligned} \tag{43}$$

In this way, $F(x, y)$ can be replaced by $\mathcal{F}(\bar{x}, \bar{y})$.

Proof: The Hessian matrix of $F(x, y)$ can be expressed as

$$\bigtriangledown^2 F(x, y) = \frac{e^{x - y}}{(1 + e^{x - y})^2 \ln 2} \begin{bmatrix} 1 & -1 \\ -1 & 1 \end{bmatrix} \succeq \mathbf{0}. \tag{44}$$

Due to the fact that the Hessian matrix of $F(x, y)$ is positive semi-definite, this bivariate function is convex with respect to x and y. According to the Taylor series approximation, it satisfies the following inequality with any given $\bar{x}$ and $\bar{y}$.

$$\begin{aligned} F(x, y) \geq \mathcal{F}(\bar{x}, \bar{y}) = &\log_2\left(1 + e^{\bar{x} - \bar{y}}\right) + \frac{e^{\bar{x} - \bar{y}}}{(1 + e^{\bar{x} - \bar{y}})\ln 2} \\ &\times (x - \bar{x} - y + \bar{y}). \end{aligned} \tag{45}$$

Similarly, the approximation in (45) holds with the conditions $\{x = \bar{x}, y = \bar{y}\}$ satisfied. In this way, (42) can be replaced by (43). ∎

Thus, according to Proposition 2, we substitute auxiliary variables $\{z_{M_i^n}[n], v_{M_i^n}[n]\}$ into x and y in (43), respectively. (31) can be transformed as a convex constraint as

$$\begin{aligned} &\log_2\left(1 + e^{\bar{z}_{M_i^n}[n] - \bar{v}_{M_i^n}[n]}\right) + \frac{e^{\bar{z}_{M_i^n}[n] - \bar{v}_{M_i^n}[n]}}{(1 + e^{\bar{z}_{M_i^n}[n] - \bar{v}_{M_i^n}[n]})\ln 2} \\ &\times \left(z_{M_i^n}[n] - \bar{z}_{M_i^n}[n] - v_{M_i^n}[n] + \bar{v}_{M_i^n}[n]\right) \geq m_{M_i^n}[n]. \end{aligned} \tag{46}$$

Based on the above derivations, **P1** has been transformed into convex one (47) at the top of this page, which can be solved by CVX.

B. Subproblem 2: UAV Trajectory Optimization

With the optimized transmit power $\mathbf{P}$ from solving (47), the optimization problem in (24) can be decomposed as

$$\begin{aligned} \mathbf{P2}: \min_{\mathbf{X}, \Delta_t} \quad & \Delta_t && \text{(48a)} \\ s.t. \quad & M_i^n \in \mathbf{M}^*, i \in \mathcal{S}, n \in \mathcal{N}, && \text{(48b)} \\ & x_u[1] = x_b, x_u[N] = x_e, && \text{(48c)} \\ & \left|x_u[n+1] - x_u[n]\right| \leq V_{max}\Delta_t, n \in \mathcal{N} - \{N\}, && \text{(48d)} \\ & \sum_n R_{M_i^n}[n]\Delta_t \geq I_{th}, (i, n) \in \mathcal{W}_k, \forall k \in \mathcal{K}. && \text{(48e)} \end{aligned}$$

P2 cannot be solved directly due to the non-convexity of the constraint (48e). Similar to approximating **P1**, we utilize SCA to transform it.

First, according to $\mathbf{M}^*$ by Algorithm 1, (48e) can be transformed as

$$R_{M_i^n}[n] \geq \zeta \frac{I_{th}}{\text{card}(\mathcal{W}_{M_i^n})\Delta_t}, M_i^n \in \mathcal{M}^{n*}, \forall n \in \mathcal{N}. \tag{49}$$

$$
\begin{aligned}
&\min_{\mathbf{P},\Delta_t} \ \Delta_t \\
&s.t. \quad M_i^n \in \mathbf{M}^*, i \in \mathcal{S}, n \in \mathcal{N}, \\
&\quad \frac{\rho_0 P_{M_i^n}[n]}{H^2+\left(x_u[n]-x_{M_i^n}\right)^2+y_{M_i^n}^2} \geq e^{\bar{z}_{M_i^n}[n]}\left(z_{M_i^n}[n]-\bar{z}_{M_i^n}[n]+1\right), M_i^n \in \mathcal{M}^{n*}, \forall n \in \mathcal{N}, \\
&\quad 1+\sum_{j=i+1}^{S} \frac{\rho_0 P_{M_j^n}[n]}{H^2+\left(x_u[n]-x_{M_j^n}\right)^2+y_{M_j^n}^2} \leq e^{\bar{v}_{M_i^n}[n]}\left(v_{M_i^n}[n]-\bar{v}_{M_i^n}[n]+1\right), M_i^n \in \mathcal{M}^{n*}, \forall n \in \mathcal{N}, \\
&\quad \log_2\left(1+e^{\bar{z}_{M_i^n}[n]-\bar{v}_{M_i^n}[n]}\right)+\frac{e^{\bar{z}_{M_i^n}[n]-\bar{v}_{M_i^n}[n]}}{\left(1+e^{\bar{z}_{M_i^n}[n]-\bar{v}_{M_i^n}[n]}\right)\ln 2} \times \left(z_{M_i^n}[n]-\bar{z}_{M_i^n}[n]-v_{M_i^n}[n]+\bar{v}_{M_i^n}[n]\right) \geq m_{M_i^n}[n], \\
&\quad \frac{1}{\Delta_t} \leq \frac{m_{M_i^n}[n]\mathrm{card}(\mathcal{W}_{M_i^n})}{\zeta I_{th}}, M_i^n \in \mathcal{M}^{n*}, \forall n \in \mathcal{N}, \\
&\quad 0 \leq P_{M_i^n}[n] \leq P_{max}, \forall i \in \mathcal{S}, \forall n \in \mathcal{N}.
\end{aligned} \tag{47}
$$

By introducing some auxiliary variables as $\{m_{M_i^n}[n], \forall M_i^n \in \mathcal{M}^{n*}\}$, (49) can be approximated as

$$R_{M_i}[n] \geq m_{M_i}[n], \tag{50}$$

$$m_{M_i^n}[n] \geq \zeta \frac{I_{th}}{\mathrm{card}(\mathcal{W}_{M_i^n})\Delta_t}. \tag{51}$$

Similar to (29), the constraint (51) can be transformed into a convex one as

$$\frac{1}{\Delta_t} \leq \frac{m_{M_i^n}[n]\mathrm{card}(\mathcal{W}_{M_i^n})}{\zeta I_{th}}, M_i^n \in \mathcal{M}^{n*}, \forall n \in \mathcal{N}. \tag{52}$$

Accordingly, we rewrite (50) as

$$\log_2\left(1+\frac{\dfrac{\rho_0 P_{M_i^n}[n]}{H^2+\left(x_u[n]-x_{M_i^n}\right)^2+y_{M_i^n}^2}}{\displaystyle\sum_{j=i+1}^{S}\frac{\rho_0 P_{M_j^n}[n]}{H^2+\left(x_u[n]-x_{M_j^n}\right)^2+y_{M_j^n}^2}+1}\right) \geq m_{M_i^n}[n]. \tag{53}$$

Similar to (32)-(34), we introduce auxiliary variables $\{z_{M_i^n}[n], v_{M_i^n}[n], \forall M_i^n \in \mathcal{M}^{n*}\}$ to approximate (53). As a result, it can be transformed as

$$\frac{\rho_0 P_{M_i^n}[n]}{H^2+\left(x_u[n]-x_{M_i^n}\right)^2+y_{M_i^n}^2} \geq e^{z_{M_i^n}[n]}, \forall n, \tag{54}$$

$$1+\sum_{j=M_{i+1}^n}^{M_S^n} \frac{\rho_0 P_j[n]}{H^2+\left(x_u[n]-x_{M_j^n}\right)^2+y_{M_j^n}^2} \leq e^{v_{M_i^n}[n]}, \tag{55}$$

$$\log_2\left(1+e^{z_{M_i^n}[n]-v_{M_i^n}[n]}\right) \geq m_{M_i^n}[n], \forall n. \tag{56}$$

In the trajectory optimization, the UAV instantaneous position $\mathbf{q}[n]$ is a variable. Thus, (54) can be transformed as

$$\frac{H^2}{\rho_0 P_{M_i^n}[n]}+\frac{\left(x_u[n]-x_{M_i^n}\right)^2+y_{M_i^n}^2}{\rho_0 P_{M_i^n}[n]} \leq e^{-z_{M_i^n}[n]}, \forall n. \tag{57}$$

Based on Proposition 2 and Proposition 3, these three constraints can be approximated as

$$\frac{H^2+\left(x_u[n]-x_{M_i^n}\right)^2+y_{M_i^n}^2}{\rho_0 P_{M_i^n}[n]} \leq e^{-\bar{z}_{M_i^n}[n]}\left(1-z_{M_i^n}[n]+\bar{z}_{M_i^n}[n]\right), \tag{58}$$

$$\begin{aligned}
1+\sum_{j=i+1}^{S}&\frac{\rho_0 P_{M_j^n}[n]}{H^2+\left(x_u[n]-x_{M_j^n}\right)^2+y_{M_j^n}^2} \\
&\leq e^{\bar{v}_{M_i^n}[n]}\left(v_{M_i^n}[n]-\bar{v}_{M_i^n}[n]+1\right),
\end{aligned} \tag{59}$$

$$\begin{aligned}
&\log_2\left(1+e^{\bar{z}_{M_i^n}[n]-\bar{v}_{M_i^n}[n]}\right)+\frac{e^{\bar{z}_{M_i^n}[n]-\bar{v}_{M_i^n}[n]}}{(1+e^{\bar{z}_{M_i^n}[n]-\bar{v}_{M_i^n}[n]})\ln 2} \\
&\times\left(z_{M_i^n}[n]-\bar{z}_{M_i^n}[n]-v_{M_i^n}[n]+\bar{v}_{M_i^n}[n]\right) \geq m_{M_i^n}[n].
\end{aligned} \tag{60}$$

However, (59) is still a non-convex constraint and cannot be solved. We further utilize auxiliary variables $\{s_{M_i^n}[n], y_{M_i^n}[n], \forall M_i^n \in \mathcal{M}^{n*}\}$ to approximate it. Assume that the distance between the UAV and ground devices satisfies

$$s_{M_i^n}[n] \leq H^2+\left(x_u[n]-x_{M_i^n}\right)^2+y_{M_i^n}^2. \tag{61}$$

Accordingly, (59) can be transformed as the following two constraints.

$$\frac{\rho_0 P_{M_i^n}[n]}{s_{M_i^n}[n]} \geq y_{M_i^n}[n], \tag{62}$$

$$1+\sum_{j=i+1}^{S} y_{M_j^n}[n] \leq e^{\bar{v}_{M_i^n}[n]}\left(v_{M_i^n}[n]-\bar{v}_{M_i^n}[n]+1\right). \tag{63}$$

Based on the Taylor series approximation and Proposition 1, the above non-convex constraints (61)-(63) can be approximated into convex ones as

$$\begin{aligned}
s_{M_i^n}[n] \leq H^2+y_{M_i^n}^2&+\left(\bar{x}_u[n]-x_{M_i^n}\right)^2 \\
&+2\left(\bar{x}_u[n]-x_{M_i^n}\right)\left(x_u[n]-\bar{x}_u[n]\right),
\end{aligned} \tag{64}$$

$$\frac{\rho_0 P_{M_i^n}[n]}{\bar{s}_{M_i^n}[n]}-\frac{\rho_0 P_{M_i^n}[n]}{\bar{s}_{M_i^n}^2[n]}\left(s_{M_i^n}[n]-\bar{s}_{M_i^n}[n]\right) \geq y_{M_i^n}[n], \tag{65}$$

$$1+\sum_{j=i+1}^{S} y_{M_j^n}[n] \le e^{\bar{v}_{M_i^n}[n]}\left(v_{M_i^n}[n]-\bar{v}_{M_i^n}[n]+1\right). \quad (66)$$

Thus, the original non-convex constraint (59) can be approximated by (64)-(66). As a result, all the non-convex constraints are transformed into convex ones via SCA, and **P2** can be transformed into a convex one as (67) at the top of the next page, which can be solved by CVX.

C. Alternating Optimization Algorithm

In Section IV-A and Section IV-B, the problem (24) has been transformed into two convex subproblems, i.e., (47) and (67). Thus, we propose an iterative algorithm to solve them. After each iteration, $\mathbf{M}^*$ is updated by Algorithm 1 accordingly. Thus, the original problem (23) can be solved iteratively by Algorithm 2.

Algorithm 2 Alternating Optimization Algorithm for (23)

1: Initialize the UAV straight trajectory $\mathbf{X}^0$ and the transmit power $\mathbf{P}^0$, set the index of iteration $r=1$.
2: **Repeat**
3: For $\mathbf{X}^r$, update $\mathbf{M}^*$ via Algorithm 1.
4: For $\mathbf{X}^r$, solve (47) using CVX to get the optimized values $\mathbf{P}^{r+1}$.
5: Using $\mathbf{P}^{r+1}$, solve (67) using CVX to get the optimized values $\mathbf{X}^{r+1}$.
6: $r=r+1$.
7: **Until** Convergence or the maximum number of iterations is satisfied.

In addition, the performance of Algorithm 2 relies on the initial UAV trajectory $\mathbf{X}^0$, which is set uniformly in the proposed scheme as

$$x_u^0[n]=x_b+\frac{(n-1)(x_e-x_b)}{N-1}, n\in\mathcal{N}. \quad (68)$$

The convergence of Algorithm 2 is shown in *Remark 2*.

Remark 2: For given $\{\mathbf{X}^r,\mathbf{P}^r\}$, the solution $\{\mathbf{X}^r,\mathbf{P}^{r+1}\}$ obtained in the $(r+1)$th iteration by solving (47) is locally optimal and the objective value is non-decreasing with iterations. In the scheme, the objective value of (47) obtained by Step 4 in Algorithm 2 is a lower bound of that in its original problem (25). Similarly, the objective value of (67) is also a lower bound of that in its original problem (48). Due to the convexity of (47) and (67), each subproblem can be solved to obtain a unique solution in each iteration. Furthermore, the objective value of (23) is upper bounded by a finite value. Therefore, Algorithm 2 can be guaranteed to converge to at least a locally optimal solution.

After the solution is calculated, it should be spread among ground devices. Nevertheless, the solution can be reused again and again if the locations of devices are unchanged, and the initialization will only be taken before the first flight.

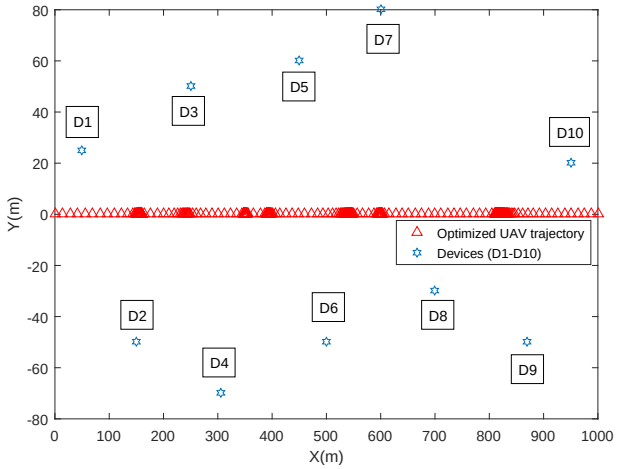

Fig. 2. The optimized UAV trajectory with 10 ground devices in the proposed scheme. $N=400$, $S=3$, $H=150$ m and $I_{th}=100$ bit/Hz. The optimized $\Delta_t^*=0.4543$ s.

D. Computational Complexity Analysis

The complexity of alternating optimization based algorithm includes the complexity of updating $\mathbf{M}^*$ in Algorithm 1, and the complexity of solving problems (47) and (67). First, the inner loop of Algorithm 1 executes $K\times N$ times, which results in the complexity of $\mathcal{O}(KN)$. Then, it is worth noticing that (47) and (67) in each iteration of Algorithm 2 are both linear programming (LP). According to [37], the complexity of solving a LP is $\mathcal{O}\left(n_L^2 m_L\right)$, where n_L denotes the dimension of optimization variables and m_L represents the number of optimization constraints. Specifically, we have $n_L=4KN$ and $m_L=(4S+K)N$ for (47). Thus, the complexity of solving (47) can be obtained as $\mathcal{O}\left(L_{P1}((4S+K)(4K)^2N^3\right)$, where L_{P1} denotes the number of iterations. Similarly, let L_{P2} denote the number of iterations required for solving (67), and the corresponding complexity can be given by $\mathcal{O}\left(L_{P2}(5S+K)(5K+1)^2N^3\right)$. Therefore, the overall computational complexity of Algorithm 2 can be represented as (69) at the top of the next page, where L_{AO} is the number of iterations required by Algorithm 2 to converge.

IV. Simulation Results and Discussion

In this section, simulation results are presented to evaluate the performance of the proposed UAV-assisted data collection scheme via uplink NOMA. We set $\beta_0=10^{-5}$, $\sigma^2=-110$ dBm, $V_{max}=30$ m/s, $P_{max}=1$ mW. The minimum data transmission threshold at all devices is assumed to be $I_{th}=100$ bit/Hz. The predefined locations of UAV are $x_b=0$ and $x_e=1000$ in meters. The relaxation factor $\zeta=0.98$. For simplicity, we denote the kth device as $D_k, k=1,2,\ldots,K$, and the total number of ground devices is $K=10$. We set $H=150$ m to guarantee the high LoS probability according to [38].

The optimized UAV trajectory with ground devices in the proposed scheme is presented in Fig. 2. We set $K=10$, $S=3$ and $N=400$. The final optimized value of time duration Δ_t^* is 0.4543s, which can be calculated by Algorithm 2. From the results, we can see that the original uniform speed

$$
\begin{aligned}
\min_{\mathbf{X},\Delta_t}\ & \Delta_t \\
s.t.\ \ & M_i^n \in \mathbf{M}^*, i \in \mathcal{S}, n \in \mathcal{N}, \\
& x_u[1] = x_b, x_u[N] = x_e, \\
& \left|x_u[n+1] - x_u[n]\right| \le V_{max}\Delta_t, n = 1, 2, \ldots, N-1, \\
& \frac{H^2 + \left(x_u[n] - x_{M_i^n}\right)^2 + y_{M_i^n}^2}{\rho_0 P_{M_i^n}[n]} \le e^{-\bar{z}_{M_i^n}[n]}\left(1 - z_{M_i^n}[n] + \bar{z}_{M_i^n}[n]\right), M_i^n \in \mathcal{M}^{n*}, \forall n \in \mathcal{N}, \\
& s_{M_i^n}[n] \le H^2 + y_{M_i^n}^2 + \left(\bar{x}_u[n] - x_{M_i^n}\right)^2 + 2\left(\bar{x}_u[n] - x_{M_i^n}\right)^T (x_u[n] - \bar{x}_u[n]), M_i^n \in \mathcal{M}^{n*}, \forall n \in \mathcal{N}, \\
& 1 + \sum_{j=i+1}^{S} y_{M_j^n}[n] \le e^{\bar{v}_{M_i^n}[n]}\left(v_{M_i^n}[n] - \bar{v}_{M_i^n}[n] + 1\right), M_i^n \in \mathcal{M}^{n*}, \forall n \in \mathcal{N}, \\
& \frac{\rho_0 P_{M_i^n}[n]}{\bar{s}_{M_i^n}[n]} - \frac{\rho_0 P_{M_i^n}[n]}{\bar{s}_{M_i^n}^2[n]}\left(s_{M_i^n}[n] - \bar{s}_{M_i^n}[n]\right) \ge y_{M_i^n}[n], M_i^n \in \mathcal{M}^{n*}, \forall n \in \mathcal{N}, \\
& \log_2\left(1 + e^{\bar{z}_{M_i^n}[n] - \bar{v}_{M_i^n}[n]}\right) + \frac{e^{\bar{z}_{M_i^n}[n] - \bar{v}_{M_i^n}[n]}}{\left(1 + e^{\bar{z}_{M_i^n}[n] - \bar{v}_{M_i^n}[n]}\right)\ln 2} \times \left(z_{M_i^n}[n] - \bar{z}_{M_i^n}[n] - v_{M_i^n}[n] + \bar{v}_{M_i^n}[n]\right) \ge m_{M_i^n}[n], \\
& \frac{1}{\Delta_t} \le \frac{m_{M_i^n}[n]\mathrm{card}(\mathcal{W}_{M_i^n})}{\zeta I_{th}}, M_i^n \in \mathcal{M}^{n*}, \forall n \in \mathcal{N}.
\end{aligned}
\tag{67}
$$

$$
\mathcal{O}\left(L_{AO}\left(KN + L_{P1}(4S+K)(4K)^2N^3 + L_{P2}(5S+K)(5K+1)^2N^3\right)\right). \tag{69}
$$

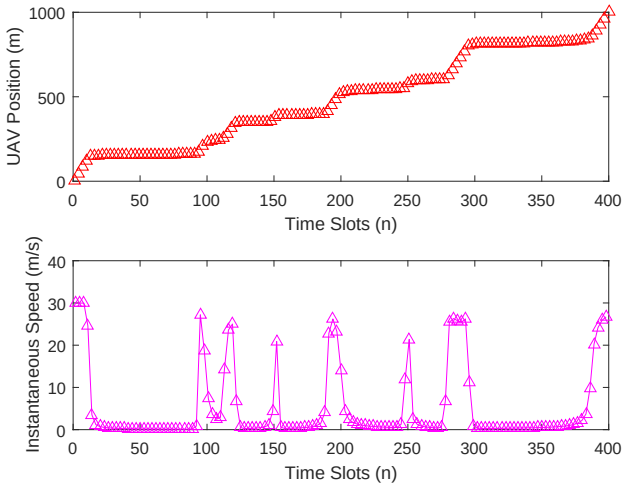

Fig. 3. The optimized UAV position and instantaneous speed in the proposed scheme. $N = 400$, $S = 3$, $H = 150$ m and $I_{th} = 100$ bit/Hz.

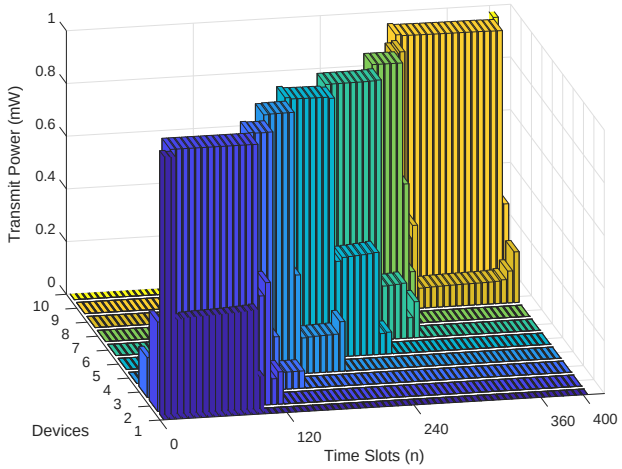

Fig. 4. The optimized transmit power for each device over slots in the proposed scheme. $N = 400$, $S = 3$, $H = 150$ m and $I_{th} = 100$ bit/Hz.

trajectory in (68) is optimized as in Fig. 2. The sparse parts of the trajectory show the UAV flies at a high speed, while the dense parts of the trajectory indicate that, the speed of UAV is slow down at these locations to guarantee that the UAV can collect enough data from the devices. To illustrate this further, the optimized position and instantaneous speed of the UAV in the proposed scheme with the same parameters are shown in Fig. 3. From the results, we can observe that during the flight, the instantaneous speed of UAV is optimized to change between zero and V_{max}, which satisfies the mobility constraint of UAV. Particularly, the time slots that the UAV flies at a low speed correspond to the dense parts in Fig. 2. Furthermore, the proposed scheme is also valid with more devices, the result of which is similar and omitted here for simplicity.

In Fig. 4, the optimized transmit power of each device with $N = 400$, $S = 3$, $H = 150$ m, and $I_{th} = 100$ bit/Hz in the proposed scheme is presented. From the results, we can see that the transmit power is varying over slots, due to the fact that the location of the UAV is changing. Accordingly, the accessible devices and $\mathcal{M}^n$ are also changing in each time slot. In order to maximize the transmission rate, the accessible device with better channel gain is optimized to upload data at higher power. Particularly, the different transmit power indicates different SIC decoding orders in each time slot.

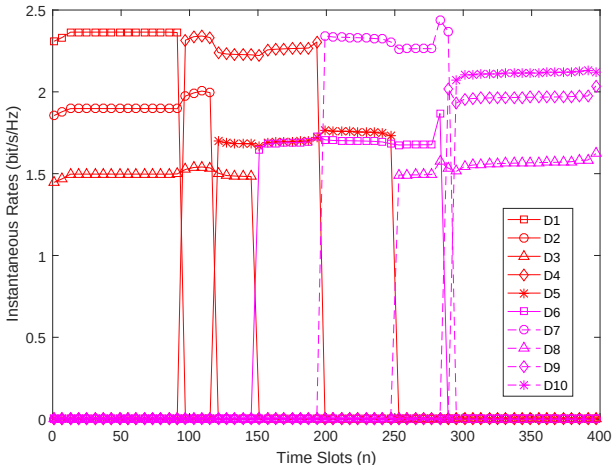

Fig. 5. The optimized instantaneous rates for different devices with $N = 400$, $S = 3$, $H = 150$ m and $I_{th} = 100$ bit/Hz in the proposed scheme.

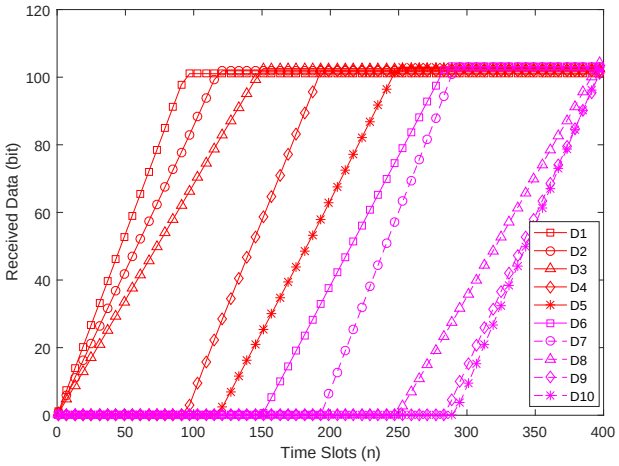

Fig. 6. The collected data from ground devices with $N = 400$, $S = 3$, $H = 150$ m and $I_{th} = 100$ bit/Hz in the proposed scheme.

The accessible device with a higher channel gain transmits at higher power with its information decoded first. Furthermore, the optimized instantaneous rates for different devices with the same parameters are compared in Fig. 5. From the results, we can observe that only three devices can access the uplink NOMA network in each time slot, and the instantaneous rates of all accessible devices are high.

The collected data from all ground devices with $N = 400$, $S = 3$, $H = 150$ m and $I_{th} = 100$ bit/Hz in the uplink NOMA scheme are compared in Fig. 6. From the results, we can see that the collected data from the devices increase with time slots. At last, the amount of data collected from each device is higher than I_{th}. In addition, the moment that the collected data from a certain device starts to grow indicates that this device is connected to the uplink NOMA network at this time slot, while the collected data from one device remains constant means that the device is out of the network.

To further evaluate the performance of the proposed NOMA scheme, we introduce a frequency-division multiple access (FDMA) data collection scheme. For bandwidth split $\mu_{M_i^n} \in [0, 1]$, assume that 1 Hz bandwidth is divided equally for

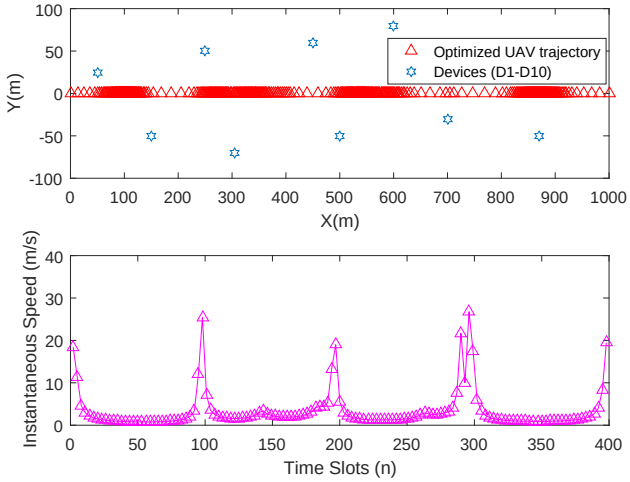

Fig. 7. The optimized UAV trajectory and instantaneous speed of the UAV with $N = 400$, $S = 3$, $H = 150$ m and $I_{th} = 100$ bit/Hz in the FDMA scheme. The optimized $\Delta_t^* = 0.5188$ s.

S accessible devices, e.g., $\mu_{M_i^n} = \frac{1}{S}$. Then, the achievable transmission rate of the FDMA scheme from the M_i^nth device to the UAV in the nth time slot in bit/second/Hertz can be formulated by

$$R_{M_i^n}^{FD}[n] = \mu_{M_i^n} \log_2 \left(1 + \frac{P_{M_i^n}[n] \left|h_{M_i^n}[n]\right|^2}{\mu_{M_i^n} \sigma^2}\right). \quad (70)$$

Then, the optimization problem in the FDMA scheme can be formulated as

$$\begin{aligned} \min_{\mathbf{P},\mathbf{X},\Delta_t} \quad & \Delta_t \\ s.t. \quad & M_i^n \in \mathbf{M}^*, i \in \mathcal{S}, n \in \mathcal{N}, \\ & \sum_n R_{M_i^n}^{FD}[n]\Delta_t \geq I_{th}, (i,n) \in \mathcal{W}_k, \forall k \in \mathcal{K}, \\ & x_u[1] = x_b, x_u[N] = x_e, \\ & \left|x_u[n+1] - x_u[n]\right| \leq V_{max}\Delta_t, n \in \mathcal{N} - \{N\}, \\ & 0 \leq P_{M_i^n}[n] \leq P_{max}, \forall i \in \mathcal{S}, \forall n \in \mathcal{N}. \end{aligned} \quad (71)$$

The approximations and solutions for (71) are similar to the proposed NOMA scheme. The designed device scheduling strategy is also suitable for the FDMA scheme.

The optimized UAV trajectory and instantaneous speed of the UAV in the FDMA scheme are compared in Fig. 7. $N = 400$, $S = 3$, $H = 150$ m and $I_{th} = 100$ bit/Hz. From the results, we can observe that with the FDMA scheme, the optimized trajectory has longer length of dense parts compared with that of the proposed NOMA scheme in Fig. 2. It indicates that the UAV needs to slow down over lots of time slots to collect enough data because of the lower achievable rate in the FDMA scheme compared with that of the proposed NOMA scheme, which results in the longer Δ_t^* and T_{total}^*.

To further demonstrate the effectiveness of the proposed uplink NOMA scheme, we consider the optimized duration of each time slot Δ_t^* and optimized total time T_{total}^* with different data transmission threshold I_{th} in Fig. 8. Without loss of generality, four situations have been discussed, i.e., the FDMA scheme with uniform speed, the FDMA scheme with joint optimization, the NOMA scheme with uniform

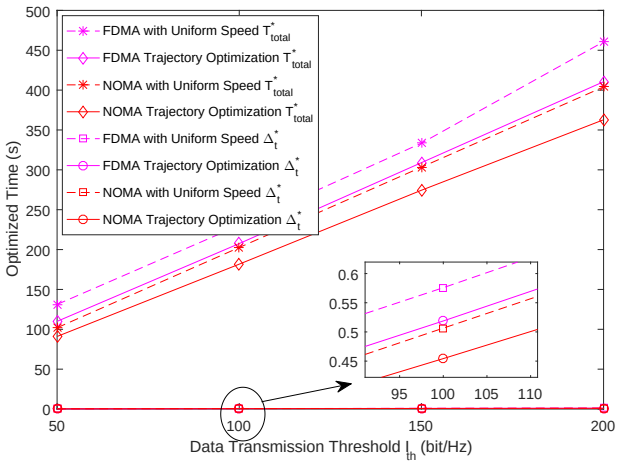

Fig. 8. The optimized duration of each time slot Δ_t^* and optimized total time T_{total}^* with different values of I_{th} for different schemes. $N = 400$, $S = 3$ and $H = 150$ m.

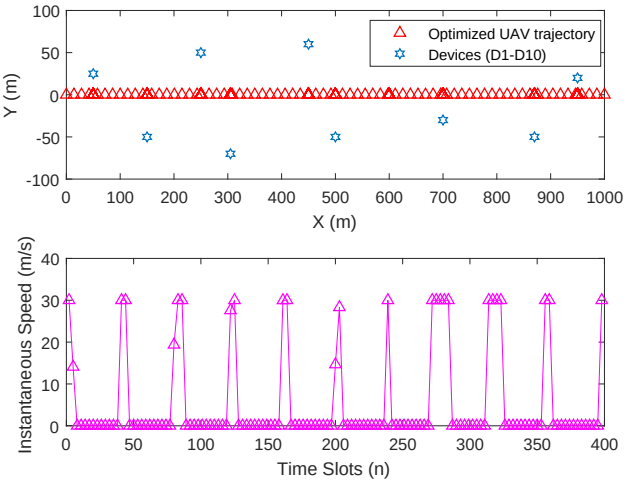

Fig. 9. The optimized UAV trajectory and instantaneous speed of the UAV with $N = 400$, $S = 1$, $H = 150$ m and $I_{th} = 100$ bit/Hz in the TDMA scheme. The optimized $\Delta_t^* = 0.4689$ s.

speed, the NOMA scheme with joint optimization. $N = 400$, $S = 3$ and $H = 150$ m. From the results, we can observe that the optimized Δ_t^* and the optimized T_{total}^* increase with the growth of I_{th}. When the threshold I_{th} is fixed, the optimized Δ_t^* and T_{total}^* in the proposed NOMA scheme are always shorter than other three schemes. In addition, it is worth noticing that when the threshold I_{th} increases, the gap between the NOMA scheme and the FDMA scheme is gradually widening, which verifies the superiority of NOMA-UAV data collection from ground devices.

Furthermore, the optimized UAV trajectory and instantaneous speed of the UAV in the time-division multiple access (TDMA) scheme are compared in Fig. 9. $N = 400$, $S = 1$, $H = 150$ m and $I_{th} = 100$ bit/Hz. The optimized $\Delta_t^* = 0.4689$ s, which is worse than that of the proposed NOMA scheme. From the results, we can observe that with the TDMA scheme, the optimized trajectory has more dense parts compared with that of the proposed NOMA scheme in Fig. 2. It means that when the UAV flies close to each device, the speed of UAV is slow down accordingly such that enough

TABLE I
THE OPTIMIZED Δ_t^* FOR DIFFERENT NUMBER OF ACCESSIBLE DEVICES

Number of accessible devices	Access technology	Optimized Δ_t^*
$S = 3$	NOMA	0.4543 s
$S = 2$	NOMA	0.4614 s
$S = 1$	TDMA	0.4689 s

data can be uploaded to the UAV over a better LoS link. This phenomenon can be also observed from the change of UAV speed in Fig. 9. The speed of UAV first reduces to zero when it flies close to a device, after it collects enough data, the speed switches quickly to V_{max} in order to get close to the next device.

In addition, the optimized Δ_t^* for different number of accessible devices S with $N = 400$, $H = 150$ m and $I_{th} = 100$ bit/Hz is compared in Table I. Particularly, when $S = 1$, the proposed NOMA scheme reduces to the TDMA scheme. From the results, we can observe that increasing the number of accessible devices S leads to a shorter Δ_t^*, which means that the data collection at the UAV is faster and more efficient. However, a larger S compromises the instantaneous uplink rate for each device, due to the stronger multiple-access interference and more complex SIC. Furthermore, in practical NOMA systems, the number of accessible devices in each time slot should not be very large to avoid the imperfect SIC. Thus, it is suitable for us to set $S = 2$ or $S = 3$ in practical systems.

V. Conclusions and Future Work

In this paper, we have proposed a UAV-assisted uplink NOMA scheme to achieve time-efficient data collection from ground devices. The total flight time is equally divided into N time slots, and the duration of each time slot is minimized by jointly optimizing the straight-line trajectory, device scheduling, and transmit power. Due to the non-convexity of the optimization problem, we have decomposed it into two steps. First, we propose a device scheduling strategy based on the straight-line trajectory and the channel gains between the UAV and devices. Then, the optimal duration of each time slot can be obtained by two subproblems, i.e., the transmit power optimization and the UAV trajectory optimization. Each subproblem is first converted into convex by applying SCA, then solved by an iterative algorithm with the device scheduling updated at the end of each iteration. Simulation results show that the NOMA scheme requires less time than the FDMA and TDMA schemes, and the proposed scheduling strategy and optimization can significantly reduce the operation time. In addition, the proposed scheme is mathematically applicable to the 2D trajectory design. However, when the network scale is large and the ground devices are scattered, the proposed algorithm for the 2D trajectory design fails to converge occasionally. The possible reason is that under such circumstances, the UAV has to fly a longer distance and the instantaneous device-UAV distance is varying, resulting in a varying decoding order of NOMA. In the future work, improved algorithms will be explored to fully release the potential of UAV trajectory design for data collection via NOMA. Furthermore, the user clustering and

the path discretization method will be considered to improve the efficiency.

ACKNOWLEDGEMENT

We thank the editor and reviewers for their detailed reviews and constructive comments, which have greatly improved the quality of this paper.

REFERENCES

[1] W. Wang, N. Zhao, L. Chen, X. Liu, Y. Chen, and D. Niyato, "Time-efficient uplink data collection for UAV-assisted NOMA networks," in *Proc. IEEE WCNC'21*, pp. 1–6, Nanjing, China, Mar. 2021.

[2] Y. Zeng, R. Zhang, and T. J. Lim, "Wireless communications with unmanned aerial vehicles: opportunities and challenges," *IEEE Commun. Mag.*, vol. 54, no. 5, pp. 36–42, May. 2016.

[3] W. Mei, Q. Wu, and R. Zhang, "Cellular-connected UAV: Uplink association, power control and interference coordination," *IEEE Trans. Wireless Commun.*, vol. 18, no. 11, pp. 5380–5393, Nov. 2019.

[4] X. Pang, G. Gui, N. Zhao, W. Zhang, Y. Chen, Z. Ding, and F. Adachi, "Uplink precoding optimization for NOMA cellular-connected UAV networks," *IEEE Trans. Commun.*, vol. 68, no. 2, pp. 1271–1283, Feb. 2020.

[5] J. Lyu, Y. Zeng, R. Zhang, and T. J. Lim, "Placement optimization of UAV-mounted mobile base stations," *IEEE Commun. Lett.*, vol. 21, no. 3, pp. 604–607, Mar. 2017.

[6] S. Gong, S. Wang, C. Xing, S. Ma, and T. Q. S. Quek, "Robust superimposed training optimization for UAV assisted communication systems," *IEEE Trans. Wireless Commun.*, vol. 19, no. 3, pp. 1704–1721, Mar. 2020.

[7] T. Zhang, Y. Xu, J. Loo, D. Yang, and L. Xiao, "Joint computation and communication design for UAV-assisted mobile edge computing in IoT," *IEEE Trans. Ind. Informat.*, vol. 16, no. 8, pp. 5505–5516, Aug. 2020.

[8] N. C. Luong, D. T. Hoang, P. Wang, D. Niyato, D. I. Kim, and Z. Han, "Data collection and wireless communication in internet of things (IoT) using economic analysis and pricing models: A survey," *IEEE Commun. Surveys Tuts.*, vol. 18, no. 4, pp. 2546–2590, 4th Quart. 2016.

[9] C. Zhan, Y. Zeng, and R. Zhang, "Energy-efficient data collection in UAV enabled wireless sensor network," *IEEE Wireless Commun. Lett.*, vol. 7, no. 3, pp. 328–331, Jun. 2018.

[10] J. Gong, T. Chang, C. Shen, and X. Chen, "Flight time minimization of UAV for data collection over wireless sensor networks," *IEEE J. Sel. Areas Commun.*, vol. 36, no. 9, pp. 1942–1954, Sept. 2018.

[11] M. Samir, S. Sharafeddine, C. M. Assi, T. M. Nguyen, and A. Ghrayeb, "UAV trajectory planning for data collection from time-constrained IoT devices," *IEEE Trans. Wireless Commun.*, vol. 19, no. 1, pp. 34–46, Jan. 2020.

[12] Z. Ding, X. Lei, G. K. Karagiannidis, R. Schober, J. Yuan, and V. K. Bhargava, "A survey on non-orthogonal multiple access for 5G networks: Research challenges and future trends," *IEEE J. Sel. Areas Commun.*, vol. 35, no. 10, pp. 2181–2195, Oct. 2017.

[13] Z. Shi, S. Ma, H. ElSawy, G. Yang, and M. Alouini, "Cooperative HARQ-assisted NOMA scheme in large-scale D2D networks," *IEEE Trans. Commun.*, vol. 66, no. 9, pp. 4286–4302, Sept. 2018.

[14] L. Dai, B. Wang, Y. Yuan, S. Han, C. l. I, and Z. Wang, "Non-orthogonal multiple access for 5G: Solutions, challenges, opportunities, and future research trends," *IEEE Commun. Mag.*, vol. 53, no. 9, pp. 74–81, Sept. 2015.

[15] N. Rupasinghe, Y. Yapıcı, İ. Güvenç, and Y. Kakishima, "Non-orthogonal multiple access for mmwave drone networks with limited feedback," *IEEE Trans. Commun.*, vol. 67, no. 1, pp. 762–777, Jan. 2019.

[16] T. M. Nguyen, W. Ajib, and C. Assi, "A novel cooperative NOMA for designing UAV-assisted wireless backhaul networks," *IEEE J. Sel. Areas Commun.*, vol. 36, no. 11, pp. 2497–2507, Nov. 2018.

[17] W. Mei and R. Zhang, "Uplink cooperative NOMA for cellular-connected UAV," *IEEE J. Sel. Topics Signal Process.*, vol. 13, no. 3, pp. 644–656, Jun. 2019.

[18] M. Liu, G. Gui, N. Zhao, J. Sun, H. Gacanin, and H. Sari, "UAV-aided air-to-ground cooperative nonorthogonal multiple access," *IEEE Internet Things J.*, vol. 7, no. 4, pp. 2704–2715, Apr. 2020.

[19] W. Wang, J. Tang, N. Zhao, X. Liu, X. Y. Zhang, Y. Chen, and Y. Qian, "Joint precoding optimization for secure SWIPT in UAV-aided NOMA networks," *IEEE Trans. Commun.*, vol. 68, no. 8, pp. 5028–5040, Aug. 2020.

[20] N. Zhao, Y. Li, S. Zhang, Y. Chen, W. Lu, J. Wang, and X. Wang, "Security enhancement for NOMA-UAV networks," *IEEE Trans. Veh. Technol.*, vol. 69, no. 4, pp. 3994–4005, Apr. 2020.

[21] T. Z. H. Ernest, A. S. Madhukumar, R. P. Sirigina, and A. K. Krishna, "NOMA-aided UAV communications over correlated Rician shadowed fading channels," *IEEE Trans. Signal Process.*, vol. 68, pp. 3103–3116, May 2020.

[22] X. Pang, J. Tang, N. Zhao, X. Zhang, and Y. Qian, "Energy-efficient design for mmWave-enabled NOMA-UAV networks," *Sci. China Inf. Sci.*, vol. 64, no. 4: 140303, Apr. 2021.

[23] X. Chen, Z. Yang, N. Zhao, Y. Chen, J. Wang, Z. Ding, and F. R. Yu, "Secure transmission via power allocation in NOMA-UAV networks with circular trajectory," *IEEE Trans. Veh. Technol.*, vol. 69, no. 9, pp. 10033–10045, Sept. 2020.

[24] T. Hou, Y. Liu, Z. Song, X. Sun, and Y. Chen, "Exploiting NOMA for UAV communications in large-scale cellular networks," *IEEE Trans. Commun.*, vol. 67, no. 10, pp. 6897–6911, Oct. 2019.

[25] A. A. Nasir, H. D. Tuan, T. Q. Duong, and H. V. Poor, "UAV-enabled communication using NOMA," *IEEE Trans. Commun.*, vol. 67, no. 7, pp. 5126–5138, Jul. 2019.

[26] T. Hou, Y. Liu, Z. Song, X. Sun, and Y. Chen, "Multiple antenna aided NOMA in UAV networks: A stochastic geometry approach," *IEEE Trans. Commun.*, vol. 67, no. 2, pp. 1031–1044, Feb. 2019.

[27] F. Cui, Y. Cai, Z. Qin, M. Zhao, and G. Y. Li, "Multiple access for mobile-UAV enabled networks: Joint trajectory design and resource allocation," *IEEE Trans. Commun.*, vol. 67, no. 7, pp. 4980–4994, Jul. 2019.

[28] N. Zhao, X. Pang, Z. Li, Y. Chen, F. Li, Z. Ding, and M. Alouini, "Joint trajectory and precoding optimization for UAV-assisted NOMA networks," *IEEE Trans. Commun.*, vol. 67, no. 5, pp. 3723–3735, May. 2019.

[29] X. Mu, Y. Liu, L. Guo, and J. Lin, "Non-orthogonal multiple access for air-to-ground communication," *IEEE Trans. Commun.*, vol. 68, no. 5, pp. 2934–2949, May. 2020.

[30] W. Chen, S. Zhao, R. Zhang, Y. Chen, and L. Yang, "UAV-assisted data collection with non-orthogonal multiple access," *IEEE Internet Things J.*, vol. 8, no. 1, pp. 501–511, Jan. 2021.

[31] A. Al-Hourani, S. Kandeepan, and S. Lardner, "Optimal LAP altitude for maximum coverage," *IEEE Wireless Commun. Lett.*, vol. 3, no. 6, pp. 569–572, Dec. 2014.

[32] Q. Wu, J. Xu, and R. Zhang, "Capacity characterization of UAV-enabled two-user broadcast channel," *IEEE J. Sel. Areas Commun.*, vol. 36, no. 9, pp. 1955–1971, Sept. 2018.

[33] Z. Yang, Z. Ding, P. Fan, and N. Al-Dhahir, "A general power allocation scheme to guarantee quality of service in downlink and Uplink NOMA systems," *IEEE Trans. Wireless Commun.*, vol. 15, no. 11, pp. 7244–7257, Nov. 2016.

[34] R. Duan, J. Wang, C. Jiang, H. Yao, Y. Ren, and Y. Qian, "Resource allocation for multi-UAV aided IoT NOMA uplink transmission systems," *IEEE Internet Things J.*, vol. 6, no. 4, pp. 7025–7037, Aug. 2019.

[35] Y. Zeng, J. Xu, and R. Zhang, "Energy minimization for wireless communication with rotary-wing UAV," *IEEE Trans. Wireless Commun.*, vol. 18, no. 4, pp. 2329–2345, Apr. 2019.

[36] C. Zhan, H. Hu, X. Sui, Z. Liu, and D. Niyato, "Completion time and energy optimization in the UAV-enabled mobile-edge computing system," *IEEE Internet Things J.*, vol. 7, no. 8, pp. 7808–7822, Aug. 2020.

[37] S. Boyd and L. Vandenberghe, *Convex optimization*. Cambridge, U.K.:Cambridge Univ. Press, 2004.

[38] X. Lin, V. Yajnanarayana, S. D. Muruganathan, S. Gao, H. Asplund, H. Maattanen, M. Bergstrom, S. Euler, and Y. E. Wang, "The sky is not the limit: LTE for unmanned aerial vehicles," *IEEE Commun. Mag.*, vol. 56, no. 4, pp. 204–210, Apr. 2018.